Electronic Supplementary Information (ESI)

Flexible Sandwich-shaped Composite Film of Simultaneous Double Electrically Conductive Anisotropy, Magnetism and Dual-color Fluorescence

Hetian Chen, Qianli Ma, Jiao Tian, Xiaobing Li, Dan Li, Xiangting Dong*, Wensheng Yu, Jinxian Wang, Guixia Liu

Key Laboratory of Applied Chemistry and Nanotechnology at Universities of Jilin Province, Changchun University of Science and Technology, Changchun 130022

Fax: 86 0431 85383815; Tel: 86 0431 85582574; E-mail: dongxiangting888@163.com

Chemical Reagents

Aniline (ANI), (1S)-(+)10-camphorsulfonic acid (CSA), $CHCl_3$, *N,N*-dimethylformamide (DMF), methylmethacrylate (MMA), ammonium persulfate (APS), benzoylperoxide (BPO), Tb_4O_7 (99.99 %), concentrated nitric acid (HNO_3), benzoic acid (BA), 1,10-phenanthroline (phen), $FeSO_4 \cdot 7H_2O$, $FeCl_3 \cdot 6H_2O$, NH_4NO_3, oleic acid (OA), ammonia, PVP K90 (Mw≈1300000), polyethylene glycol (PEG, Mw≈20000), PAN (Mw≈85000) and absolute alcohol were purchased from Beijing Chemical Works. All the chemicals were analytically pure and directly used as received without further purification. Deionized water was made by ourselves.

Table S1 Schematic diagrams of electrospinning process and constitutional unit of five comparative specimens

Specimens	Electrospinning process	Constitutional unit
JNAF	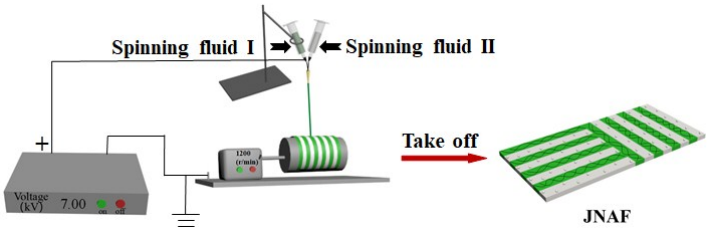	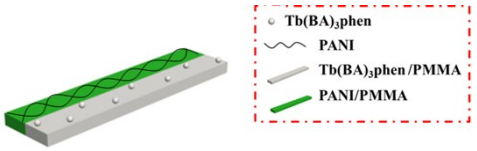
JNNF	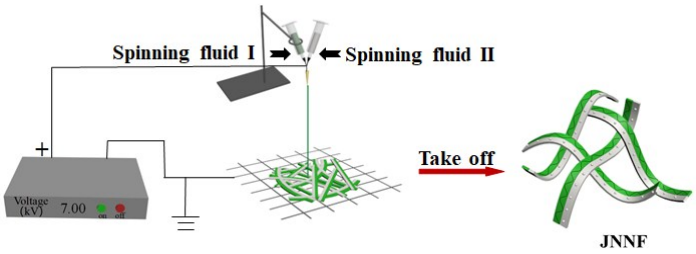	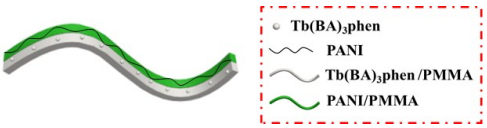
CNAF	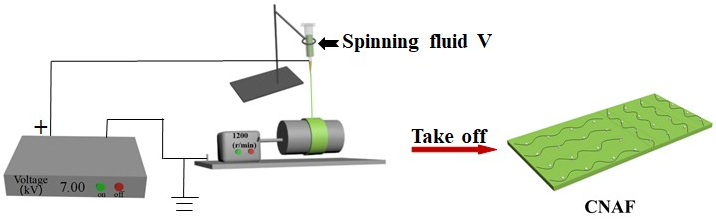	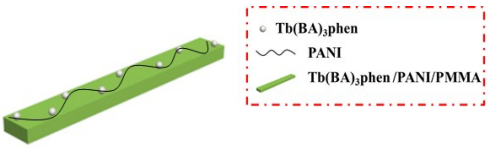
CNNF	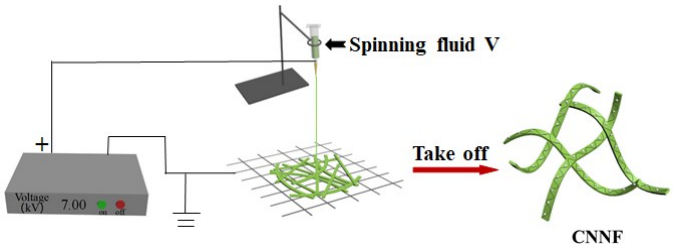	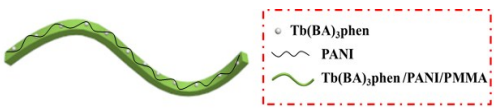

DCF

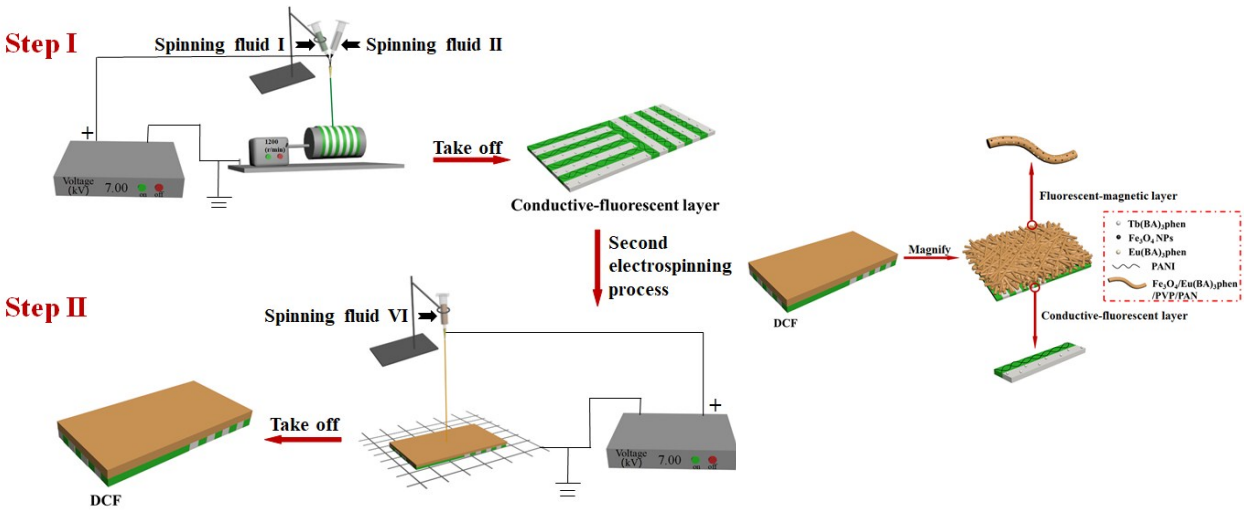

Characterisation Methods

The as-prepared Fe_3O_4 NPs, Fe_3O_4/PVP nanofibers film, SCF and DCF were identified *via* using X-ray diffractometer (XRD), the operation current and voltage were maintained at 20 mA and 40 kV, respectively. The morphology and internal structure of the products were observed by a scanning electron microscope (SEM, JSM-7610F) and optical microscope (OM, CVM500E). An energy dispersive spectrometer (EDS) produced by Oxford Instruments and attached to the SEM was used to analyze elemental compositions. The fluorescence properties of the specimens were investigated by using a Hitachi fluorescence spectrophotometer F-7000, and the excitation and emission slits were respectively 2.5 nm and 5.0 nm. The electrical conduction and the magnetization were measured by an ECOPIA HMS-3000 Hall effect measurement system and a vibrating specimen magnetometer (VSM, MPMS SQUID XL), respectively.

Observation of Morphology and Structure

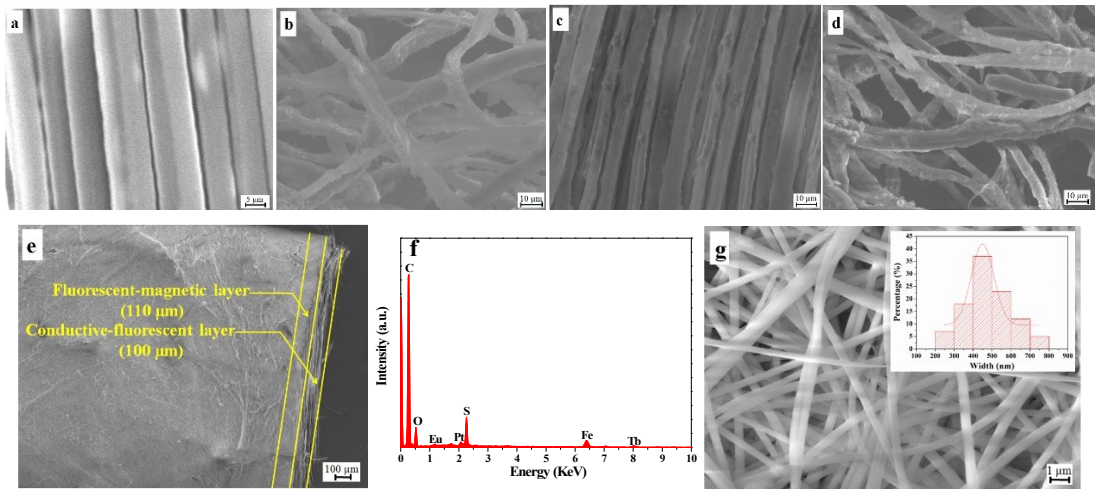

Fig. S1 SEM images of (a) JNAF, (b) JNNF, (c) CNAF and (d) CNNF; SEM images of (e) cross-section, (g) fluorescent-magnetic layer and (f) EDS spectrum of DCF; inset in (g): histograms of diameter distribution of fluorescent-magnetic layer

Electrical Conduction of Specimens

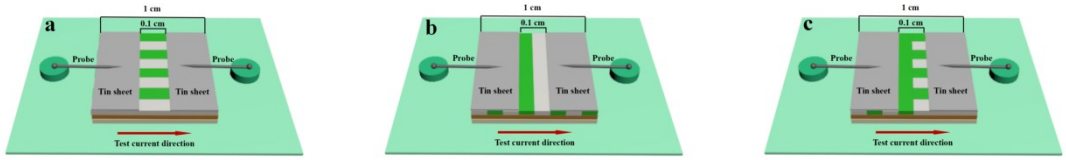

Fig. S2 Schematic of specimens conductance test: (a) parallel direction test, (b) vertical direction test and (c) LP-to-RP direction test for the first layer of SCF

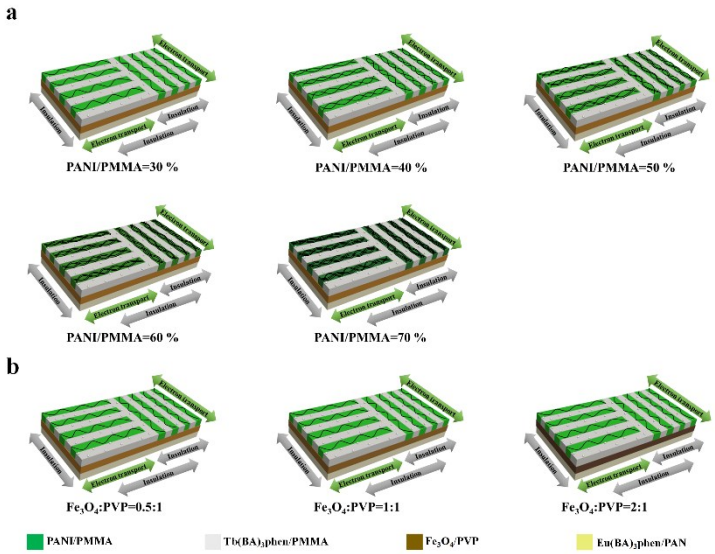

Fig. S3 Schematic diagram of SCF with different mass ratios of (a) PANI and (b) Fe_3O_4 NPs

Magnetism Analysis

As shown in Fig. S4, the saturation magnetization of the as-prepared Fe_3O_4 NPs is 61.1 emu·g^{-1} and neither remanence nor coercivity is detected.

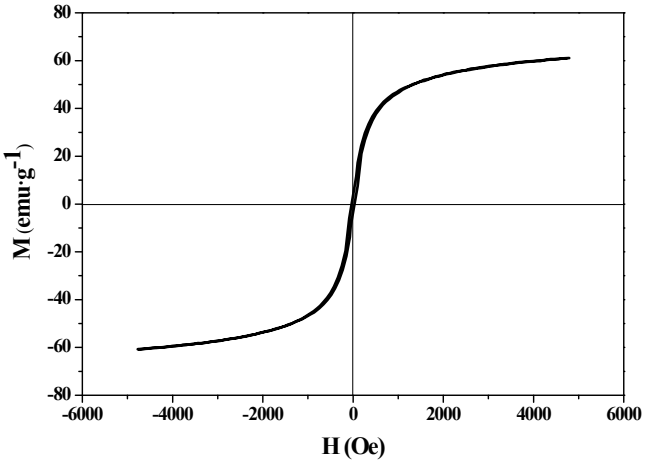

Fig. S4 Hysteresis loops of Fe_3O_4 NPs

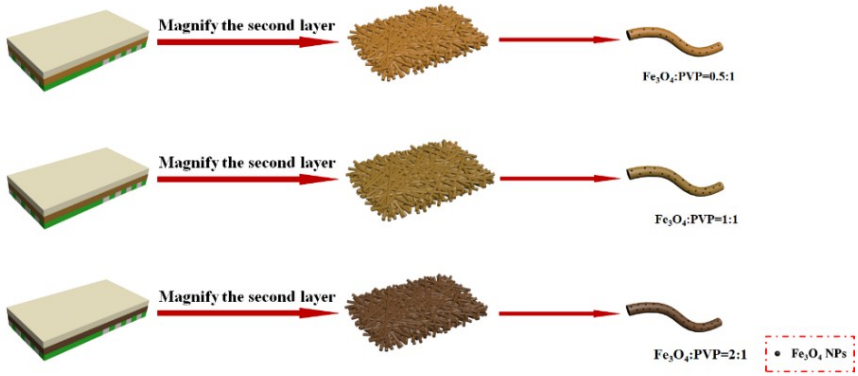

Fig. S5 Schematic diagram of the SCF with various mass ratios of Fe_3O_4 to PVP

Luminescence Characteristics

A series of Tb(BA)$_3$phen/PMMA nanoribbons doped with various percentages of Tb(BA)$_3$phen to PMMA were fabricated to find the optimal ratio of Tb(BA)$_3$phen to PMMA in the insulating-fluorescent side of the first layer of SCF. The Tb(BA)$_3$phen/PMMA nanoribbons were prepared by traditional single nozzle electrospinning process using spinning solutions F_{II-1} to F_{II-5}, respectively. The excitation and emission spectra of Tb(BA)$_3$phen/PMMA nanoribbons are provided in Fig. S6. The fluorescent intensity of Tb(BA)$_3$phen/PMMA nanoribbons increases with the increase of the concentration of Tb(BA)$_3$phen from the beginning, reaching a maximum value when the specimen is fabricated by using spinning solution F_{II-2} (10 %), and then decreases as the Tb(BA)$_3$phen concentration further increases. From the observation of the excitation spectrum (Fig. S6a), a broad excitation band extending from 200 nm to 350 nm with a strongest peak at 276 nm can be ascribed to $\pi \rightarrow \pi^*$ electron transition of ligands with a monitoring wavelength of 545 nm. Simultaneously, the characteristic emission peaks (Fig. S6b) of Tb(BA)$_3$phen are observed under 276-nm UV excitation, which are located at 489, 545, 585 and 622 nm. These peaks are respectively attributed to $^5D_4 \rightarrow {}^7F_6$ (489 nm), $^5D_4 \rightarrow {}^7F_5$ (545 nm), $^5D_4 \rightarrow {}^7F_4$ (585 nm), $^5D_4 \rightarrow {}^7F_3$ (622 nm) energy level transitions of Tb^{3+}, and the green light emission at 545 nm assigned to $^5D_4 \rightarrow {}^7F_5$ ultra-sensitive transition is primary. The results indicate that the composite nanoribbons containing 10 % of Tb(BA)$_3$phen have the strongest fluorescent intensity. Therefore, 10 % of Tb(BA)$_3$phen is adopted for fabricating the insulating-fluorescent side of the first layer of SCF in this study.

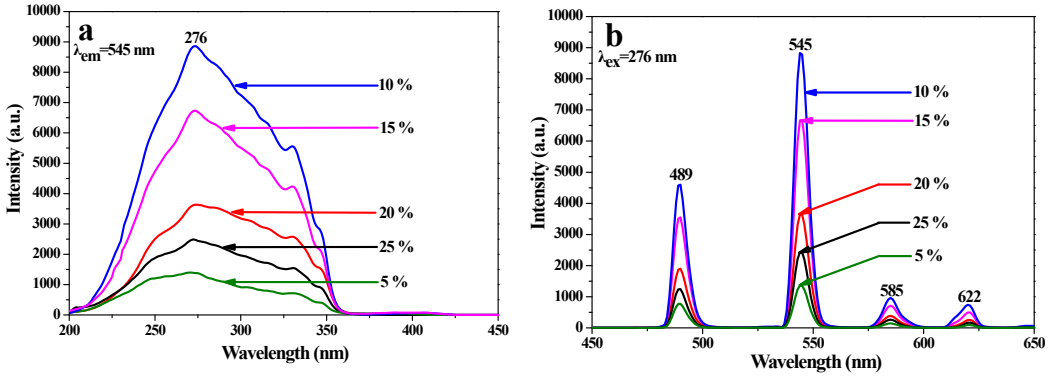

Fig. S6 (a) Excitation and (b) emission spectra of Tb(BA)$_3$phen/PMMA nanoribbons doped with different percentages of Tb(BA)$_3$phen

The same way is chosen to find the optimum percentage of $Eu(BA)_3phen$ to PAN of the third layer of SCF (spinning solutions F_{IV-1} to F_{IV-5}). As seen from the excitation spectra (Fig. S7a), a broad excitation band extending from 200 nm to 350 nm with a strongest peak at 275 nm can be ascribed to $\pi \rightarrow \pi^*$ electron transition of ligands when the monitoring wavelength is 615 nm. Meanwhile, characteristic emission peaks (Fig. S7b) of $Eu(BA)_3phen$ are observed under the excitation of 275-nm ultraviolet light, which are located at 592 and 615 nm. These peaks are respectively attributed to $^5D_0 \rightarrow {}^7F_1$ (592 nm), $^5D_0 \rightarrow {}^7F_2$ (615 nm) energy level transitions of Eu^{3+}, and the red light emission at 615 nm assigned to $^5D_0 \rightarrow {}^7F_2$ hypersensitive transition is dominant. The results imply that the composite nanofibers containing 10 % of $Eu(BA)_3phen$ have the strongest fluorescent intensity. Thus, 10 % of $Eu(BA)_3phen$ is adopted for fabricating the third layer of SCF in this study.

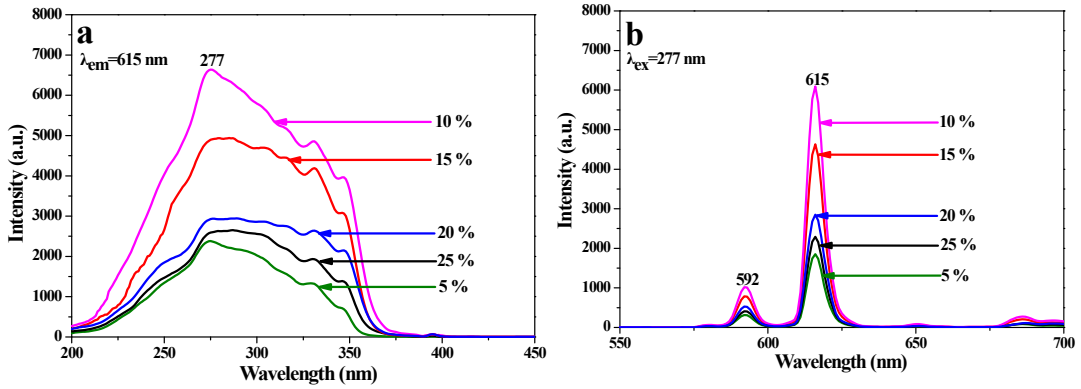

Fig. S7 Excitation and (b) emission spectra of $Eu(BA)_3phen$/PAN nanofibers doped with different percentages of $Eu(BA)_3phen$/PAN

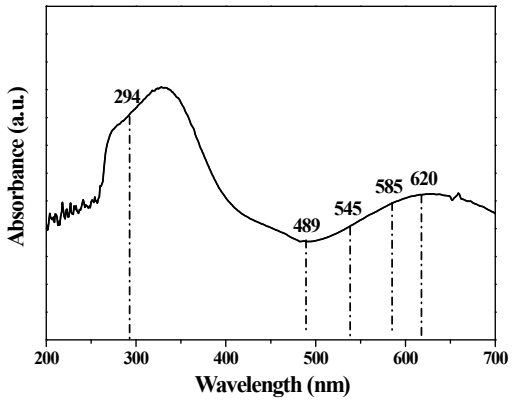

Fig. S8 UV-Vis absorbance spectrum of PANI

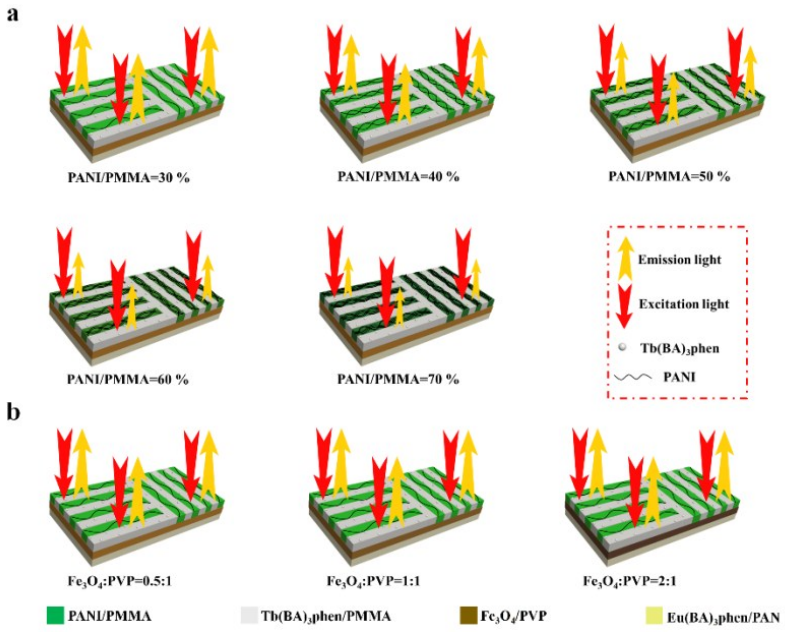

Fig. S9 Schematic illustrations of the excitation light and emission light of the first layer of SCF doped with different ratios of (a) PANI in the first layer and (b) Fe_3O_4 NPs in the second layer

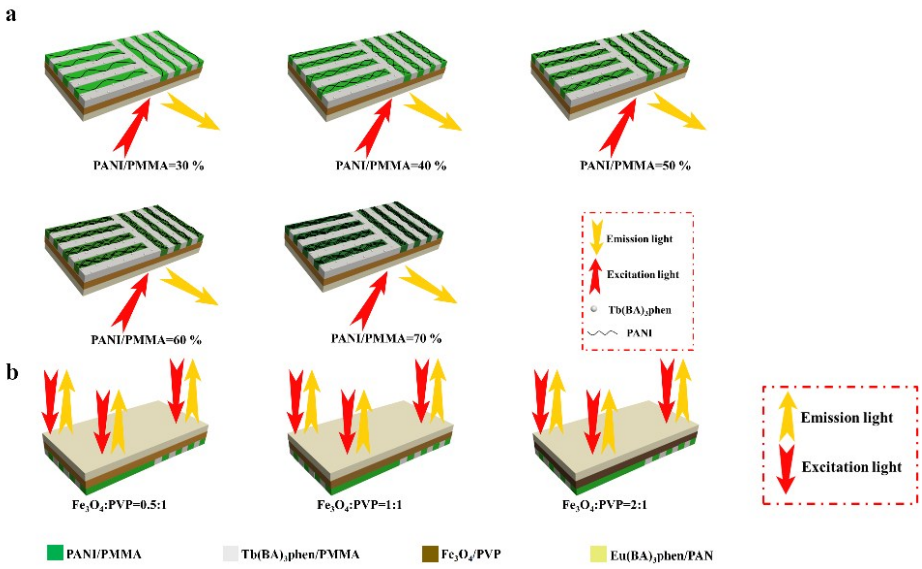

Fig. S10 Schematic diagrams of the excitation light and emission light of the third layer of SCF (a) while the first layer of SCF is doped with different ratios of PANI and (b) when the second layer of SCF is doped with different ratios of Fe_3O_4 NPs

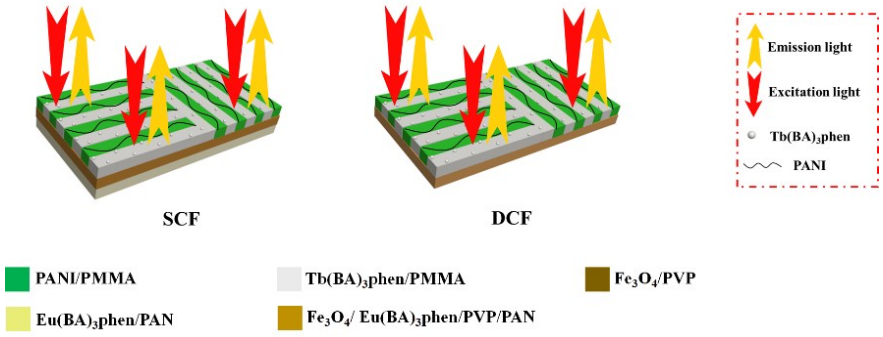

Fig. S11 Schematic diagram of the excitation light and emission light of the first layer of SCF and the conductive-fluorescent layer of DCF as comparative specimen

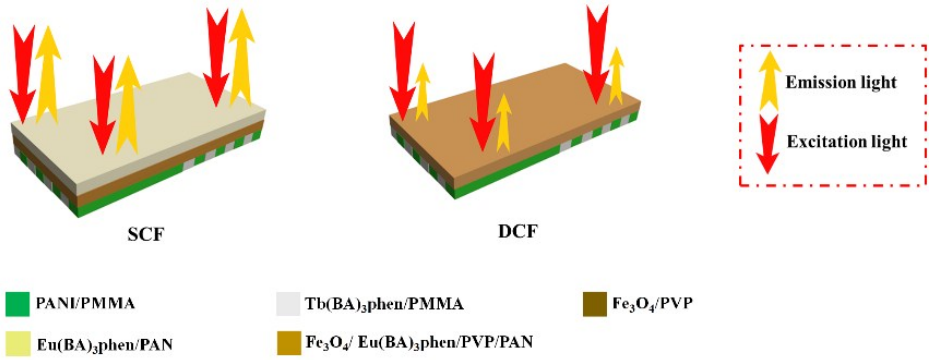

Fig. S12 Schematic diagram of the excitation light and emission light of the third layer of SCF and the fluorescent-magnetic layer of DCF as comparative specimen